Journal of Power Sources 183 (2008) 164–173

Contents lists available at ScienceDirect

Journal of Power Sources

journal homepage: www.elsevier.com/locate/jpowsour

Semi-analytical proton exchange membrane fuel cell modeling

Denver F. Cheddie [a,*], Norman D.H. Munroe [b]

[a] Department of Energy Studies, The University of Trinidad and Tobago, Pt. Lisas Campus, Esperanza Road, Brechin Castle, Couva, Trinidad and Tobago
[b] Mechanical and Materials Engineering, CEAS 2103, Florida International University, 10555W Flagler Street, Miami, FL 33174, USA

ARTICLE INFO

Article history:
Received 25 March 2008
Received in revised form 24 April 2008
Accepted 25 April 2008
Available online 4 May 2008

Keywords:
Analytical PEM fuel cell modeling
Mathematical techniques

ABSTRACT

Mathematical techniques are presented which allow for analytical solutions of the catalyst layer transport and electrochemical problem in PEM fuel cells. These techniques transform the volumetric reaction terms to boundary flux terms, thereby eliminating the need for computational solving of the catalyst layer problem. The result is a semi-analytical fuel cell model—a computational model that entails analytical rather than computational catalyst layer solutions. This helps to alleviate the meshing difficulties inherent in the catalyst layers caused by large geometric aspect ratios, and hence reduce the computational requirements for fuel cell models.

These analytical solutions are implemented in a 3D PEM fuel cell model, and the results of the semi-analytical model match well with the full computational model in terms of the polarization performance and species concentration distribution. In addition, these analytical solutions were able to reduce the required computational memory by a factor of approximately 3, and the computational time by a factor of approximately 4.

1. Introduction

Fuel cells have generated considerable interest in recent years, being heralded as the power generating devices of the future. Proton exchange membrane (PEM) fuel cells are prime candidates to eventually replace the internal combustion engine (ICE) in vehicles. They use hydrogen as fuel, which reacts electrochemically (without direct combustion) with oxygen to produce electrical power. The only emissions from a fuel cell are water and heat, thereby making them more environmentally friendly than ICEs.

Fuel cell modeling and simulation are critical aspects of the development of fuel cell technology. This is evident from the numerous publications pertaining to fuel cell modeling over the past 15 years. Fuel cell modeling has evolved from 1D to 3D [1–3], from steady state to transient, from single phase to two phases [4], and from straight channels to more complex serpentine and inter-digitated flow fields [5–8]. Our group, as well as others, were responsible for the development of intermediate to high temperature PEM fuel cell modeling using alternative membranes to Nafion®, e.g. polybenzimidazole (PBI) [9–16].

Fuel cell modeling may be divided into two categories—transport modeling and system modeling. Transport models are used when specific details of transport phenomena need to be studied. They are comprehensive; they study the relevant transport phenomena occurring within the fuel cell, and solve the governing equations in the multi-dimension space-time fuel cell domain. The level of detail and complexity often determines the required computational resources. The convergence time of a transport model may range from minutes to days depending on the level of complexity and the available computational resources, which may range from a single desktop/laptop to a parallel processing network. Transport modeling has been used to conduct parametric studies of fuel cell performance [3], and to investigate design issues such as fuel composition, water and thermal management [8], catalyst micro-structure [7], the effect of flow field geometries [5,6], and the effect of using different types of membranes [9–16].

System models, on the other hand, are used when the entire power plant containing the fuel cell stack needs to be analyzed. These models are not devoted to the detailed analysis of transport phenomena, but rather the fuel cell system as a whole, and specifically how the fuel cell interacts (sometimes in real time) with other physical and virtual components. As a result they require less computational resources. System models have been used in real time simulation and for design of control systems [17], and thus require fast computations being performed numerous times. Real time models require these computations to be performed up to 1000 times every second [18]. Control models, employing feedback loops,

Abbreviations: CL, catalyst layer; GDE, governing differential equation; GDL, gas diffusion layer; PEM, proton exchange membrane.

* Corresponding author. Tel.: +1 868 686 5369; fax: +1 868 636 3339.
E-mail addresses: denver.cheddie@utt.edu.tt (D.F. Cheddie), munroen@fiu.edu (N.D.H. Munroe).

0378-7753/$ – see front matter © 2008 Elsevier B.V. All rights reserved.
doi:10.1016/j.jpowsour.2008.04.067

Nomenclature

a	effective surface area (m^{-1}), reaction term constant
c	specific heat capacity ($J\,kg^{-1}\,K^{-1}$), constant of proportionality
$D_{i,j}$	diffusivity of gas pair i–j ($m^2\,s^{-1}$)
F	Faraday constant, 96487 $C\,mol^{-1}$
i	current density ($A\,m^{-2}$)
i_0	exchange current density ($A\,m^{-2}$)
j	reaction rate ($A\,m^{-3}$)
k	thermal conductivity ($W\,m^{-1}\,K^{-1}$), mathematical constant
m	mole fraction
M	molar mass ($kg\,mol^{-1}$)
n	reaction parameter
P	pressure (Pa)
R	reaction term, universal gas constant, 8.3143 $J\,mol^{-1}\,K^{-1}$
S	source, entropy
T	temperature (K)
u	velocity ($m\,s^{-1}$)

Greek letters

α	charge transfer coefficient
β	gas permeability (m^2)
γ	concentration parameter
ε	porosity
μ	dynamic viscosity (Pa s)
ρ	density ($kg\,m^{-3}$)
σ	electrical or ionic conductivity ($S\,m^{-1}$)
φ	electrical or ionic potential (V)

Subscripts and superscripts

e	electrolyte phase
eff	effective
i, j	species i, j
s	solid phase
T	thermal

also require numerous computations to be performed in a short space of time. So for system models, it is necessary to greatly simplify the problem in order to reduce computational requirements. Consequently, system models are usually 0D (lumped models) or 1D [19]. Essentially system models compromise detail for speed. For certain applications, especially those involving control systems, there is the need to either increase the level of detail of system models, or reduce the computational requirements of transport models. Mathematical techniques designed to reduce the computational requirements of transport models are the focus of this paper.

A purely mathematical model will require very little computer memory, since it will analytically solve the fuel cell governing equations resulting in a closed form solution. However, this is not realistic due to the highly non-linear nature of the fuel cell governing differential equations, and thus closed form mathematical solutions do not exist. A purely computational model on the other hand, does require a high amount of computer memory. Such models use finite element, finite volume or finite difference methods to approximate the real problem. Meshing is primarily responsible for the large memory requirements. Most of the models published in the open literature are computational, involving very little if any mathematical solutions. As such, very few analytical models have been reported, and the most that do are designed to be stand-alone models, not incorporated into computational models [20–25]. Litster and Djilali [26] published 1D analytical solutions of the cathode catalyst layer, which they implemented in a 2D model of an air-breathing fuel cell. Since the meshing requirements are most demanding in the catalyst region (see Figs. 1 and 2), an analytical solution of the catalyst problem incorporated into a computational model will greatly reduce the computational requirements. The present work considers both the anode and cathode catalyst layers, and implements the analytical solutions in a 3D fuel cell model.

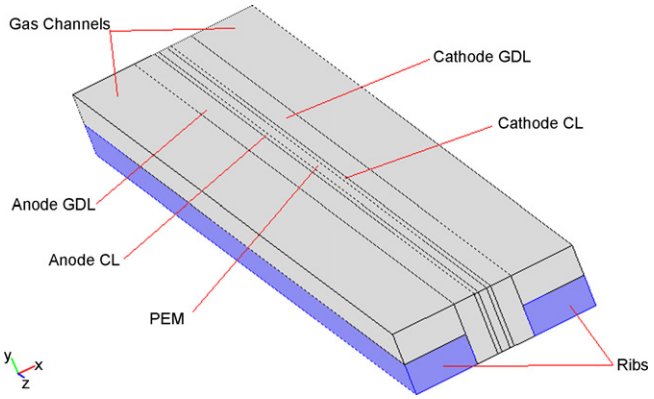

Fig. 1. PEM fuel cell regions and computational sub-domains.

2. Rationale

Meshing is difficult in a fuel cell for two reasons. First, there are very large geometric aspect ratios, since the dimensions normal to the membrane cross-section (x direction) are up to three orders of magnitude smaller than the other dimensions. Secondly, even in the x direction, there are significant scaling discrepancies, since the catalyst layer is up to two orders of magnitude thinner than the other regions. So meshing becomes very difficult, often requiring scaling to create the optimum balance between reducing memory requirements and compromising model accuracy. Fig. 1 shows a schematic of the fuel cell sub-domains. This figure depicts straight channel flow fields showing half of the channel cross-section and half of the ribs, with symmetry being assumed across the y extremes. Fig. 2 shows the same sub-domains as Fig. 1, but with the finite element mesh displayed. It shows how dense a mesh must be used in the catalyst layers.

The catalyst layer is a very thin (~10 μm) three-dimensional region sputtered with catalyst particles, and with electrochemical reaction rates varying along the thickness of the layer. Modeling

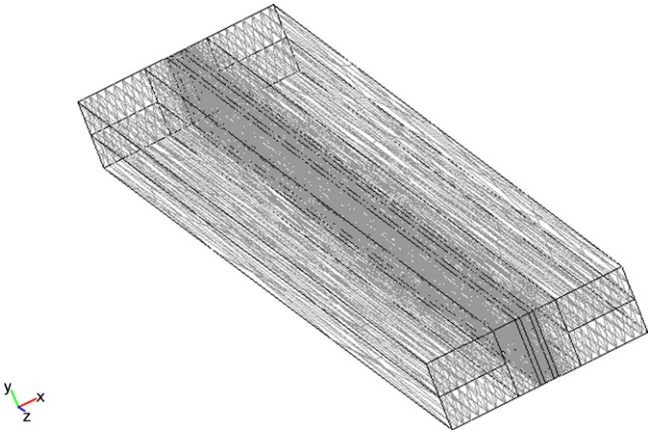

Fig. 2. 3D finite element mesh.

the CL as a finite-sized region is very demanding and much care must be taken with regards to computer memory requirements and convergence. Also, depending on the reaction rate, there may be a very high rate of species depletion on the outer surface of the catalyst region, thus confining the electrochemical reactions to an even thinner layer of the catalyst region. In such cases, an even denser mesh must be used in that ultra thin region.

Some modelers have precluded this problem by treating the catalyst region as an infinitesimally small interface, rather than a finite-sized region, all of the reaction phenomena being reckoned on this interface. Typically, the species concentration at this interface is used in the Butler–Volmer equation (or Tafel equation), for which the effective catalyst surface area must be adjusted to account for the transformation from the actual 3D porous catalyzed region to a simplified 2D catalyzed interface. One problem with this approach is that it does not account for the concentration variation that actually exists across the 3D catalyst region.

In this work, we develop mathematical solutions to the phenomena occurring in the 3D catalyst region. These solutions are used to quantify the amount of species consumption or generation, and consequently to more accurately specify the flux of species occurring at the GDL/CL interface. In other words, these techniques mathematically transform the volumetric catalyst layer source terms into interfacial boundary conditions (flux terms). This treatment precludes the problem of meshing the catalyst layer, thus reducing the computational requirements of the model, while at the same time utilizing a more accurate 3D to 2D transformation than is currently practiced.

3. Model equations

The fuel cell model consists of a highly coupled non-linear multi-physics problem involving flow in porous media, diffusion and convection of species, heat transfer, charge transfer and electrochemical reactions. These phenomena are modeled using the Navier–Stokes equations, Darcy's law, the Stefan–Maxwell equations, the heat equation, Ohm's law, and the Butler–Volmer equation. These governing differential equations (GDEs) are listed below.

$$\rho u \cdot \nabla u = -\nabla P + \nabla(\mu \nabla u) - \frac{\mu}{\beta} u \tag{1}$$

$$\nabla \cdot \left(\frac{P}{RT} u m_i - \frac{P}{RT} D_i^{\text{eff}} \nabla m_i \right) = S_i \tag{2}$$

$$\nabla \cdot (\rho c u T - \rho c k \nabla T) = S_{\text{T}} \tag{3}$$

$$\nabla \cdot i_{\text{s}} = \nabla \cdot (-\sigma_{\text{s}}^{\text{eff}} \nabla \phi_{\text{s}}) = -j \tag{4}$$

$$\nabla \cdot i_{\text{e}} = \nabla \cdot (-\sigma_{\text{e}}^{\text{eff}} \nabla \phi_{\text{e}}) = +j \tag{5}$$

where j represents the rate of proton generation, which is positive at the anode and negative at the cathode. Note in Eq. (2), the term P/RT is used for the total molar gas concentration to avoid an obfuscation of terminology, and is assumed to be locally constant, consistent with the earlier simplifications. m is the mole fraction, and S_i is the molar source term. The following source terms exist only in the catalyst layers, where electrochemical reactions take place. They quantify the consumption of oxygen and hydrogen, as well as the generation of water and heat, all as a function of the reaction rate, j.

$$j = a i_0^{\text{ref}} m_i^{\gamma_i} \left\{ \exp\left[\frac{\alpha_{\text{a}} F}{RT} \eta \right] - \exp\left[-\frac{\alpha_{\text{c}} F}{RT} \eta \right] \right\} \tag{6}$$

$$S_{\text{O}_2} = \frac{j_{\text{c}}}{4F} \tag{7}$$

$$S_{\text{H}_2} = -\frac{j_{\text{a}}}{2F} \tag{8}$$

$$S_{\text{H}_2\text{O}} = -\frac{j_{\text{c}}}{2F} \tag{9}$$

$$S_{\text{rxn}} = -j_{\text{c}} \left(\eta - \frac{T \Delta S}{n F} \right) \tag{10}$$

The boundary conditions pertinent to this paper are the conditions at the GDL/CL and the CL/PEM interfaces. Species enter the catalyst region, react, and no flow occurs across the membrane. Across the CL/PEM boundary, there is no fluid flow and no diffusion of species. This is true of PBI membranes. The Nafion® membrane does allow species crossover, especially water. Our research is primarily interested in alternative high temperature membranes, such as PBI, so our results focus on PBI fuel cells.

4. Analytical techniques

It is close to impossible to solve the full fuel cell problem using mathematical techniques alone because of the highly non-linear nature of the problem. It is possible, however, to solve it using numerical techniques, which requires extensive meshing and computational requirements, depending on the level of detail desired. This section discusses the simplifications of the physical problem necessary for a purely mathematical treatment of the catalyst layer problem, and the development of those approaches. These mathematical solutions are intended to replace the need for computational modeling of the catalyst layer. The volumetric CL source terms are transformed into interfacial boundary conditions to be specified at the GDL/CL interfaces. The end result will be a model that employs mathematical rather than computational solutions of the catalyst layer problem. This will be called a semi-analytical model and is shown schematically in Fig. 3.

When this model is implemented in a computational model, the catalyst layer sub-domains are merged with the membrane to form one larger sub-domain where all ionic transport takes place. This will minimize the error in determining the effective ionic resistance of the cell.

The following simplifications are made in order to enable mathematical solutions to the catalyst layer equations.

(1) Since the flow in the porous regions is typically dominated by diffusion, we neglect the convection terms in the catalyst layer GDEs.
(2) We assume anisotropic behavior in the catalyst region. Since the catalyst region is thin, we assume that the transport of species occurs primarily in the x direction (normal to the cross-section). Therefore, we neglect transport in the y and z directions, which enables a pseudo 1D treatment of the catalyst problem. Note that this restriction applies only in the catalyst layers and not the gas diffusion layers or the gas channels.
(3) We further assume that since the catalyst region is thin in the x direction, changes in temperature, pressure and activation overpotential occurring across the layer can be neglected. Essentially, we assume these quantities only vary in the y and z directions in the catalyst layer, and there is no interaction between state properties at different (y, z) locations, consistent with assumption (2). Again, these restrictions apply only to the catalyst layers. It should be noted that we do not assume isothermal conditions, only constant x direction temperature along the thin catalyst layer at each (y, z) location.
(4) Species concentration and reaction rates are the only parameters that vary significantly across the catalyst layer in the x direction. We do not assume constant concentration of species or constant electrochemical rates across the catalyst layer, since

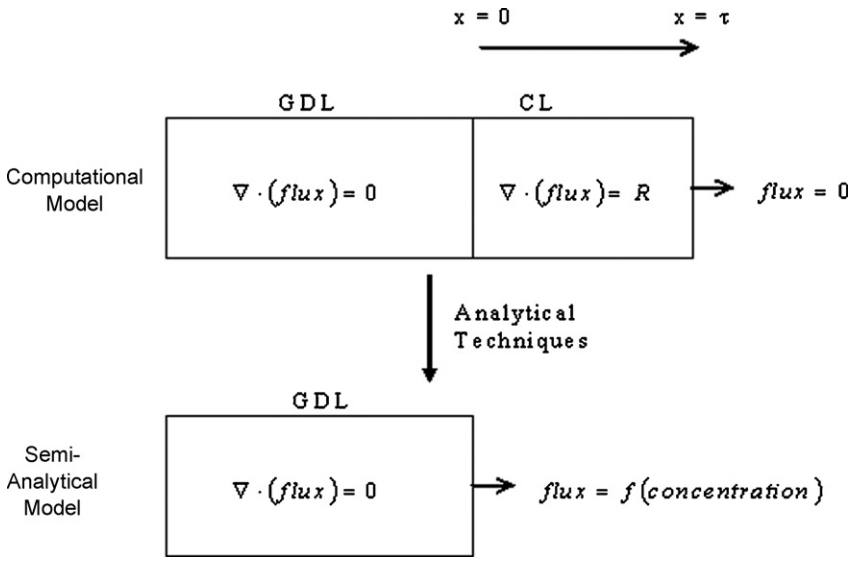

Fig. 3. Schematic and scope of the mathematical techniques presented.

assumptions of this nature are far from realistic. Instead we offer analytical solutions of the x variation in concentration at each (y, z) location.

With these assumptions, the Butler–Volmer Eq. (6) reduces to

$$j(x, y, z) = a(y, z)m(x, y, z)^n \tag{11}$$

where the species subscript, i, is dropped, and the value a is an x direction constant representing all the other terms in the Bulter–Volmer equation. From this point, the (x, y, z) notation will be dropped. The typical values for n in the PEM fuel cell are 1 (cathode) and 1/2 (anode).

We see that the volumetric reaction rate depends solely on the species concentration—hydrogen at the anode, oxygen at the cathode. Further, the species consumption source terms are linear functions of j.

$$S = -kj = -kam^n \tag{12}$$

where k is a positive constant.

The species conservation Eq. (2) in the catalyst region becomes

$$\frac{P}{RT}u\nabla m = 0 = \frac{P}{RT}D\nabla^2 m + S \tag{13}$$

or

$$\frac{\mathrm{d}^2 m}{\mathrm{d}x^2} = \left(\frac{kaRT}{PD}\right)m^n = b^2\ m^n \tag{14}$$

Eq. (14) is the simplified x direction species transport equation, which is solved at each (y, z) location. This equation is defined in the catalyst layer $(0 < x < \tau)$, where τ is the catalyst layer thickness, and x is measured from the GDL to the CL. Note that for the cathode CL, this co-ordinate is directed in the opposite direction to that shown in Figs. 1 and 2.

The concentration at $x = 0$ is known from the computational solution of the GDL problem, while insulation conditions exist at $x = \tau$. The mathematical representations of these boundary conditions are

$$m(0, y, z) = m_0(y, z) \tag{15}$$

$$\frac{\mathrm{d}}{\mathrm{d}x}m(\tau, y, z) = 0 \tag{16}$$

For the case of $n = 1$, the solution to Eq. (14) is very straightforward. For $n = 1/2$, analytical closed form solutions do not exist. Instead, we offer approximate analytical solutions based on typical conditions that often occur in PEM fuel cells. The first case is an approximation for fast reaction rates. The second case involves a Taylor series approximation to translate the power term to a linear term. The third case applies to very slow reaction rates, where the species concentration does not change significantly across the catalyst layer. These cases will then be compared for accuracy.

4.1. Case 1—fast reaction rates

When the species consumption rate is very high, the concentration quickly decreases to zero within the catalyst layer. This may happen at high current densities, or when a very active catalyst layer is present. Paradoxically, in such cases, the thin catalyst layer can be treated as infinitely large compared to the length scale of the electrochemical reaction.

Using the substitution,

$$\psi\ (m) = \frac{\mathrm{d}x}{\mathrm{d}m} \tag{17}$$

Eq. (14) becomes,

$$-\frac{1}{\psi^3}\frac{\mathrm{d}\psi}{\mathrm{d}m} = b^2\ m^n \tag{18}$$

This can be solved using separation of variables to obtain

$$\frac{1}{\psi} = \frac{\mathrm{d}m}{\mathrm{d}x} = -b\left(\frac{2m^{1+n}}{1+n}\right)^{1/2} \tag{19}$$

The constant of integration is set to zero in order to satisfy the condition that both the concentration and flux are zero when $x = \tau$. Since from Fick's law, diffusion is proportional to the negative of the first derivative of concentration, we use the negative square root in Eq. (19). From Eq. (19), we can obtain the boundary flux in terms of the mole fraction at $x = 0$.

$$\left.\frac{\mathrm{d}m}{\mathrm{d}x}\right|_{x=0} = -b\left(\frac{2m_0^{1+n}}{1+n}\right)^{1/2} \tag{20}$$

$$\left|\frac{PD}{RT}\left.\frac{\mathrm{d}m}{\mathrm{d}x}\right|_{x=0}\right| \left(\frac{2kaPDm_0^{1+n}}{RT(1+n)}\right)^{1/2} \tag{21}$$

This term represents the flux of species leaving the GDL and entering the CL at position (y, z) in terms of the species mole fraction at (y, z). This term now replaces the volumetric generation term in the catalyst region. Instead of an insulation condition being specified at the CL/PEM interface, a flux (or convection) condition is specified at the GDL/CL interface, which accounts for the electrochemical reactions occurring in the CL.

The solution can be further developed to get

$$m_0^{1-n/2} - m^{1-n/2} = \frac{a}{2^{1/2}} \frac{1-n}{(1+n)^{1/2}} x \tag{22}$$

This is valid for $0 < x < \tau$. The mole fraction, m falls to zero when

$$x = \frac{[2(1+n)]^{1/2}}{a(1-n)}\ m_0^{1-n/2} \tag{23}$$

We expect the case 1 solution to provide accurate results when the catalyst layer is larger than the RHS of Eq. (23), which provides an estimate of the thickness of the catalyst layer actually being utilized for electrochemical reactions.

All of the other source terms can be written in terms of the species source term. Suppose a particular source term is linearly related to the species source term, such that

$$S = cb^2 m^n \tag{24}$$

where c is the constant of proportionality. To find the total generation (or consumption) of that particular source term, S needs to be integrated over the catalyst region. The result would be,

$$\int_{x=0}^{\tau} S\,\mathrm{d}x = cb^2 \int_{m=m_0}^{0} m^n \frac{\mathrm{d}x}{\mathrm{d}m}\,\mathrm{d}m \tag{25}$$

$$\int_{x=0}^{\tau} S\,\mathrm{d}x = cb \int_{\omega=\omega_0}^{0} \omega^n \left(\frac{1+n}{2m^{1+n}}\right)^{1/2}\,\mathrm{d}m \tag{26}$$

$$\int_{x=0}^{\tau} S\,\mathrm{d}x = -c \left.\frac{\mathrm{d}m}{\mathrm{d}x}\right|_{x=0} \tag{27}$$

$$\int_{x=0}^{\tau} S\,\mathrm{d}x = -cb\left(\frac{2}{1+n}\right)^{1/2} m_0^{(1+n)/2} \tag{28}$$

$$\int_{x=0}^{\tau} S\,\mathrm{d}x = -c \left.\frac{\mathrm{d}m}{\mathrm{d}x}\right|_{x=0} \tag{29}$$

Not surprisingly, this is the same result that was previously obtained in Eq. (21). So all source terms (which are proportional to the species source term) can be transformed and written as linear functions of the species boundary flux with the same constants of proportionality.

4.2. Case 2—Taylor series approximations

In cases where the reactions are not fast enough to totally consume the reactants, the case 1 solution would lose accuracy. In fact, we would expect it to overestimate the reaction rate. In such cases, we may opt for an "exact" solution. If $n = 1$, the differential equation is easily solvable. For $0 < n < 1$, we can use the binomial expansion to linearize the power term, resulting in a solvable equation.

$$m^n = [1-(1-m)]^n \approx 1 - n\ (1-m) = nm + (1-n) \tag{30}$$

This approximation obviously works best when the mole fraction is close to unity, and is actually exact when $n = 1$. The solution is

$$\left.\frac{\mathrm{d}m}{\mathrm{d}x}\right|_{x=0} = bn^{1/2} \frac{1-\exp(2b\tau n^{1/2})}{1+\exp(2b\tau n^{1/2})} \left(\frac{nm_0 + 1 - n}{n}\right)$$

$$= \frac{b}{n^{1/2}} \frac{1-\exp(2b\tau n^{1/2})}{1+\exp(2b\tau n^{1/2})} m_0^n \tag{31}$$

$$\left|\frac{PD}{RT}\frac{\mathrm{d}m}{\mathrm{d}x}\right|_{x=0} = \left(\frac{kaPD}{nRT}\right)^{1/2} \frac{1-\exp(2b\tau n^{1/2})}{1+\exp(2b\tau n^{1/2})} m_0^n \tag{32}$$

4.3. Case 3—slow reaction rates

If the reaction rates are very slow, the concentration of the species does not vary significantly across the catalyst layer. This is sometimes the case with hydrogen. Since the reaction rate constant for the oxidation of hydrogen is significantly faster than the rate of oxygen reduction, the latter is the rate controlling step. So although the hydrogen is readily available for reaction, hydrogen only reacts at a rate necessary to provide a sufficient supply of protons for the oxygen reaction. This rate is much less than the rate at which hydrogen is capable of reacting, and as a result the hydrogen concentration does not vary significantly in the x direction across the catalyst layer. In such cases, we may assume that the concentration is constant across the catalyst layer. The amount of species that reacts, which is the same as the amount that diffuses across the interface, is simply

$$\left|\frac{PD}{RT}\frac{\mathrm{d}m}{\mathrm{d}x}\right|_{x=0} = -ka\tau m_0^n \tag{33}$$

4.4. Summary of all cases

At the anode, $n = 1/2$, and at the cathode, $n = 1$.

$$a = ai_0^{\mathrm{ref}} \left|\exp\left(\frac{\alpha_a E}{RT}\eta\right) - \exp\left(-\frac{\alpha_c F}{RT}\eta\right)\right| \tag{34}$$

$$k^{\mathrm{anode}} = \frac{1}{2F} \tag{35}$$

$$k^{\mathrm{cathode}} = \frac{1}{4F} \tag{36}$$

The following quantities represent the boundary condition at the GDL/CL interface that replace the volumetric CL source terms.

Case 1:

$$\mathrm{flux}(\mathrm{H_2}) = \left(\frac{4kaPD_{\mathrm{H_2}}}{3RT}\right)^{1/2} m_{\mathrm{H_2}}^{3/4} \tag{37}$$

$$\mathrm{flux}(\mathrm{O_2}) = \left(\frac{kaPD_{\mathrm{O_2}}}{RT}\right)^{1/2} m_{\mathrm{O_2}} \tag{38}$$

Case 2:

$$\mathrm{flux}(\mathrm{H_2}) = -\frac{1-\exp[\tau(2kaRT/PD_{\mathrm{H_2}})^{1/2}]}{1+\exp[\tau(2kaRT/PD_{\mathrm{H_2}})^{1/2}]} \left(\frac{2kaPD_{\mathrm{H_2}} m_{\mathrm{H_2}}}{RT}\right)^{1/2} \tag{39}$$

$$\mathrm{flux}(\mathrm{O_2}) = -\frac{1-\exp[2\tau(kaRT/PD_{\mathrm{O_2}})^{1/2}]}{1+\exp[2\tau(kaRT/PD_{\mathrm{O_2}})^{1/2}]} \left(\frac{kaPD_{\mathrm{O_2}}}{RT}\right)^{1/2} m_{\mathrm{O_2}} \tag{40}$$

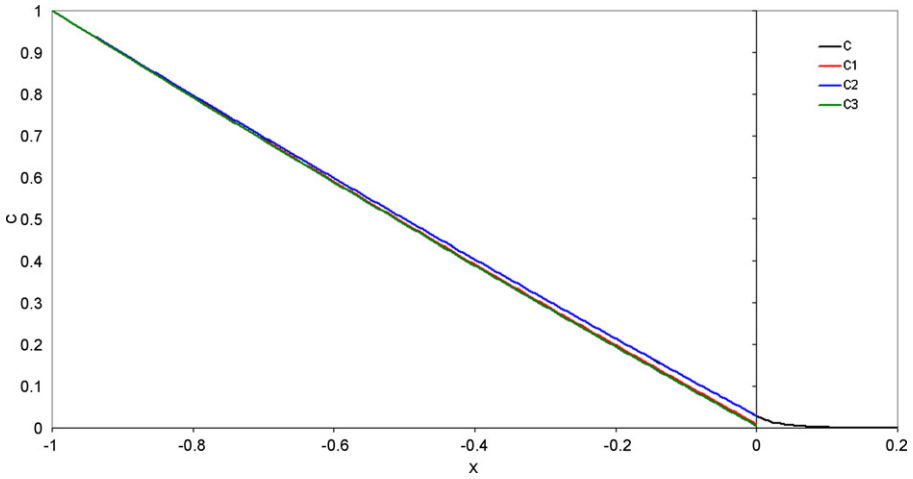

Fig. 4. Concentration profile for 1D validation ($a = 10^{-3}$, $n = 1$).

Case 3:

$$\text{flux}(H_2) = ka\tau m_{H_2}^{1/2} \tag{41}$$

$$\text{flux}(O_2) = ka\tau m_{O_2} \tag{42}$$

The remaining boundary conditions can be written as linear factors of the hydrogen and oxygen fluxes. i_a and i_c are respectively, the electronic-to-ionic current transfer at the anode and the ionic-to-electronic current transfer at the cathode. q is the heat of reaction evaluated at the cathode GDL/CL interface.

$$\text{flux}(H_2O) = -2\,\text{flux}(O_2) \tag{43}$$

$$i_a = 2F\,\text{flux}(H_2) \tag{44}$$

$$i_c = 4F\,\text{flux}(O_2) \tag{45}$$

$$q_{rxn} = \left(\eta - \frac{T\,\Delta S}{n\,F}\right)\ i_c \tag{46}$$

5. Results and discussion

The formulations derived in Section 4 are now tested for validation. First they will be applied to a simple 1D convection–conduction problem with a source term. Secondly, they will be applied to a full 3D model of a PEM fuel cell equipped with a PBI membrane.

5.1. Validation with a simplified problem

Consider a simplified conduction–convection problem governed by species conservation and Darcy's law. All units are consistent with the SI system, although not very important in this simplified example.

$$-10^{-6}\frac{d^2C}{dx^2} + u\frac{dC}{dx} = R \tag{47}$$

$$\frac{du}{dx} = -10^{-4}\frac{d^2P}{dx^2} = R \tag{48}$$

where,

$$R = \begin{Bmatrix} 0, & -1 < x < 0 \\ -aC^n, & 0 < x < 0.2 \end{Bmatrix} \tag{49}$$

The boundary conditions are

$$C(-1) = 1 \tag{50}$$

$$P(-1) = 10^5 \tag{51}$$

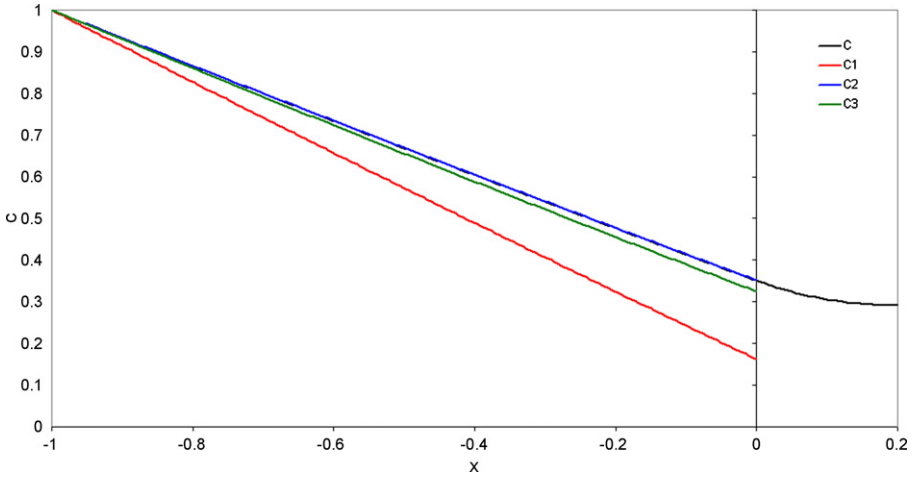

Fig. 5. Concentration profile for 1D validation ($a = 10^{-5}$, $n = 1$).

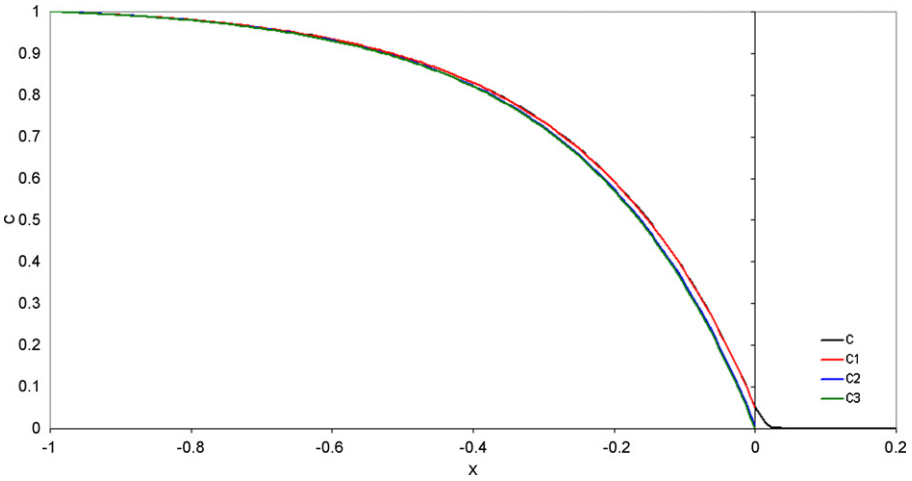

Fig. 6. Concentration profile for 1D validation ($a = 10^{-3}$, $n = 1/2$).

$$\frac{\mathrm{d}}{\mathrm{d}x}C(0.2) = 0 \tag{52}$$

$$\frac{\mathrm{d}}{\mathrm{d}x}P(0.2) = 0 = u(0.2) \tag{53}$$

This is first solved using a finite element approach with the reaction region ($0 < x < 0.2$) meshed and the spatial source term, R applied. This full computational solution is called C. It is then solved using the analytical catalyst layer treatment described in Section 4. These solutions, presented for cases 1, 2 and 3, are respectively called C1, C2 and C3. The two quantities that are varied are a and n. a represents the rate of reaction term—a high value representing a fast reaction rate, and n represents the order of the reaction.

Consider the case when $n = 1$ and $a = 10^{-3}$ (Fig. 4). This represents a fast reaction rate—evident by the fact that the concentration C falls to zero within the catalyst region ($0 < x < 0.2$). C2 matches almost exactly with C, while C1 and C3 slightly underestimate the concentration. With $n = 1$, C2 provides an exact solution to the catalyst layer equations. Therefore, it is not surprising that it accurately simulates C.

Setting $a = 10^{-5}$, which represents a slower reaction rate, results in an exaggeration of this result. Again, and expectedly as Fig. 5 shows, C2 matches almost exactly with C. Now C1 and C3 underestimate the concentration by an even greater amount. This is expected since C1 works best when the reaction rate is fast. Thus, the higher the value of a, the better is the accuracy of C1. In both cases, C3 has a small error. C3 assumes a constant concentration across the catalyst layer which is not the case in this problem. As a result, it must mathematically reduce the concentration everywhere to compensate for this inaccuracy. Most PEM fuel cell models, which use an interfacial catalyst layer treatment, employ a method which more closely resembles C3 than any of the other two. Note that this formulation does not always provide accurate results.

Now setting $n = 1/2$ and $a = 10^{-3}$ (fast reaction rate), Fig. 6 shows that C1 provides the best estimate of C. C2 is only accurate when C is close to 1, which is not the case here. So C2 slightly underestimates the concentration. For similar reasons as above, C3 also underestimates the concentration. Therefore, it is not surprising that C1 provides such accurate results, since it assumes very fast reaction rates.

Setting $a = 10^{-6}$ (Fig. 7), which represents a slow reaction rate, C1 now underestimates the concentration since it imposes a higher reaction rate than is warranted. In this case, C2 and C3 provide accurate results. C2 is accurate because the concentration is close to 1, thus rendering the Taylor series approximation valid. C3 is accurate because the actual concentration, C in the catalyst region does not change significantly. For the anode reaction in PEM fuel cells, this is the most realistic scheme. So from the simplified validation test, it seems that C2 and C3 would provide the most accurate scheme for the anode reaction, while C2 appears to be the best choice at the cathode where $n = 1$.

5.2. Validation with full 3D PEM fuel cell model

These analytical formulations are now incorporated in our previous 3D computational PBI fuel cell model [12], and results are compared. The previous model is fully computational, while the new implementation is semi-analytical. All numerical constants and operating conditions remain unaltered. These constants, listed in [12], are not repeated here since they are not relevant to the findings of this paper. It is only the comparisons of the various formulations with the full computational model that is of essence. All concentration profiles are shown for an operating cell voltage of 0.3 V. The notation *HiOj* means that the case *i* formulation is used on the hydrogen side (anode), while the case *j* formulation is used at the oxygen side (cathode). H0O0 refers to the original computational model.

Fig. 8 shows the IV curve of the original computational model and five of the semi-analytical solutions. H3O2, H3O3 and H2O2 all provide a very close match with H0O0, such that they are indistinguishable from each other on the graph. Both H1O2 and H3O1 produce inaccurate results since they require that the concentration of hydrogen and oxygen, respectively, fall to zero in the catalyst layer. As a result, they both impose higher reaction rates than are warranted by the actual problem. H3O1 is interesting. At low current densities (or low reaction rates), the deviation from H0O0 is very large. However, as the current density increases, the error becomes smaller. This is expected since at higher current densities, the depletion of oxygen becomes more pronounced. It can be expected that in cases where the oxygen concentration is fully depleted, the O1 formulation would provide accurate results.

Fig. 9 shows the hydrogen mole fraction along the gas channels and gas diffusion layers for the full computational model, H0O0. The mole fraction in the anode catalyst layer is not shown for the purpose of comparisons. The mole fraction varies from an inlet of 0.963 to a lowest value of 0.961. In this case, the hydrogen concentration does not show much variation, neither in the z direction

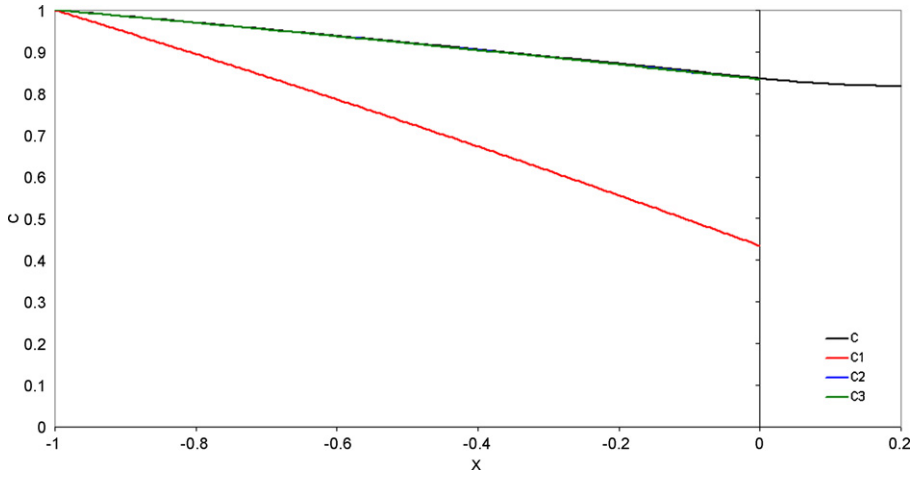

Fig. 7. Concentration profile for 1D validation ($a = 10^{-6}$, $n = 1/2$).

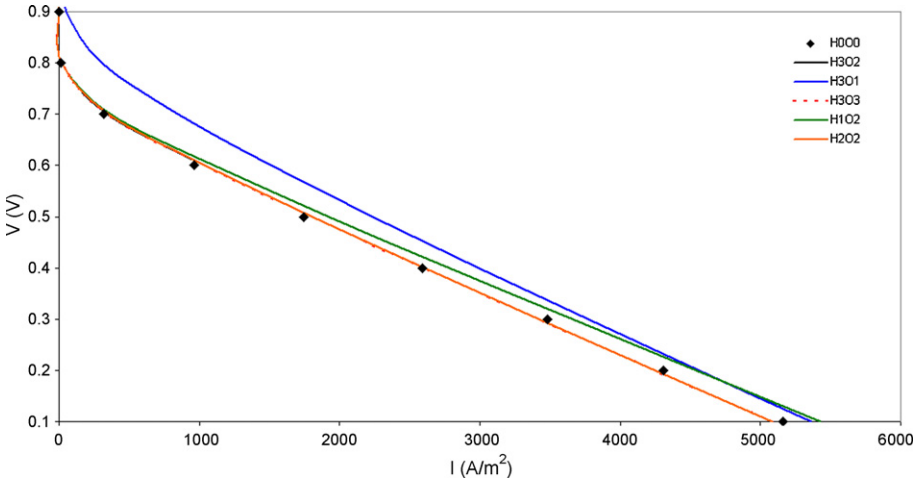

Fig. 8. Polarization curves (H000, H102, H202, H302, H301, H303).

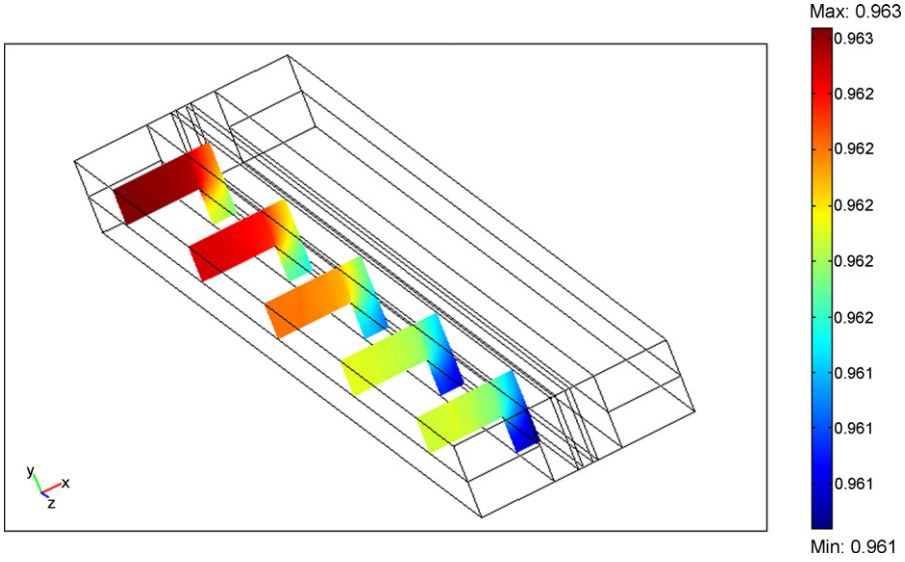

Fig. 9. Hydrogen mole fraction (H000).

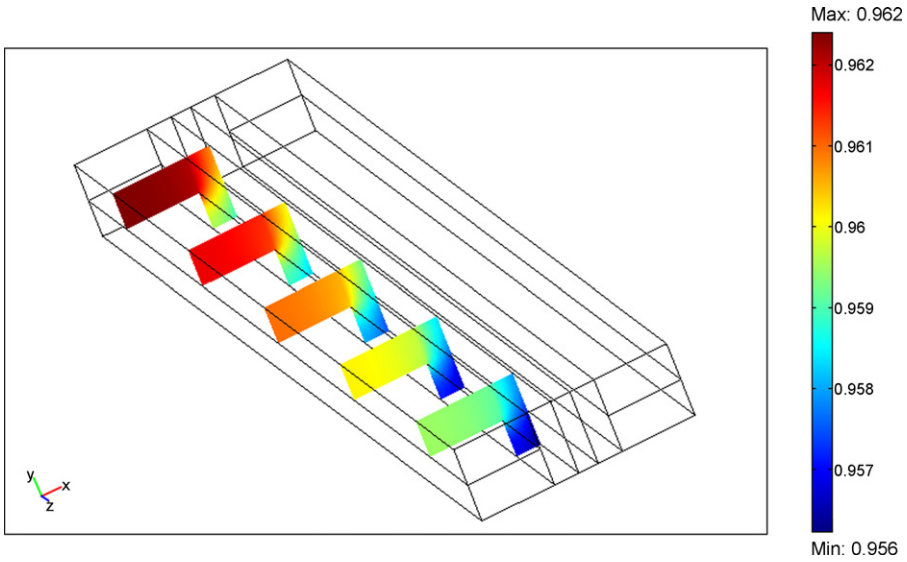

Fig. 10. Hydrogen mole fraction (H2O2, H2O3, H3O3).

nor in the *x* direction. H2O2, H3O2 and H3O3 all produce results which are barely distinguishable from each other. Consequently, only one diagram (Fig. 10) is used to display all of them. These solutions predict a similar concentration profile, but with a low mole fraction of 0.956, which is a slight deviation from the 0.961 of the computational model. However, in the context of the hydrogen concentration that does not vary significantly, this deviation is not considerable.

Fig. 11 shows the oxygen mole fraction for H0O0, with the mass fraction ranging from 0.126 to 0.194. This represents a much more significant concentration variation, as is expected with oxygen. Fig. 12 shows the equivalent plot for H2O2, H3O2 and H3O3, respectively, which as was the case with hydrogen, are indistinguishable from each other. The analytical solutions match the oxygen mole fraction almost perfectly, with the computational solution, showing virtually no difference in range or variation.

These results show that the mathematical formulations all provide a very accurate representation of the full computational model, but it greatly reduces the computational memory requirements and computation speed, since there is no need for meshing of the catalyst layer. The full computational model requires 5350 second-order tetrahedral elements, while the semi-analytical models only require 1910 finite elements. The computational model requires 24 min to gradually converge upon a solution, while the semi-analytical models require 6 min, all starting with identical initial estimates. All computations were performed on a Windows XP platform, with a 2 GHz Intel Pentium 4 processor and 512 MB RAM, using the multi-physics software FEMLAB 3.1i®.

This becomes particularly useful when dealing with larger scale models. The present model only simulated one-half channel and half rib, and assumed *y* direction symmetry. If it were required to simulate serpentine flow fields, for instance, the computational requirements would be much greater. The formulations presented here can help to reduce that requirement and allow larger problems to be modeled with less computational resources. The techniques presented here can also be applied to 2D transport models, and may simplify them enough to be used in system models involving control systems and other applications.

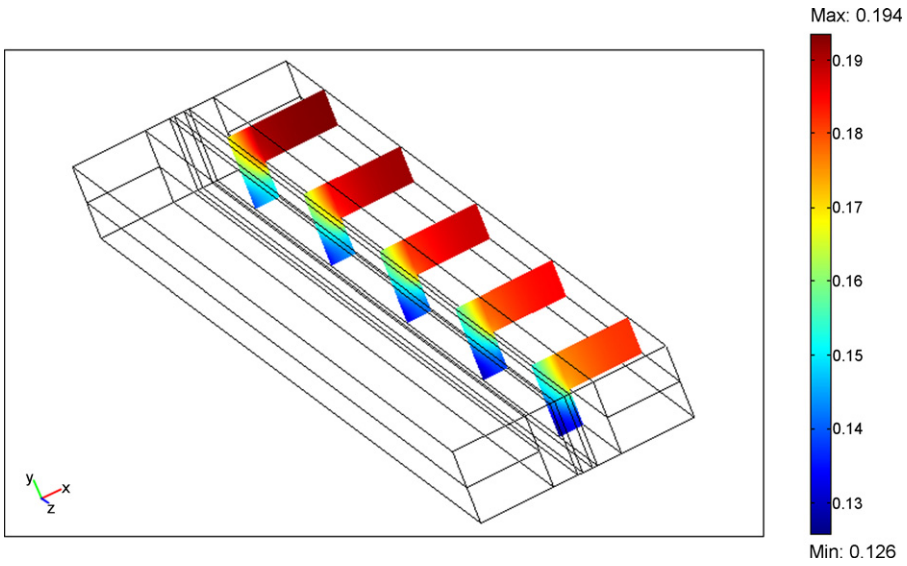

Fig. 11. Oxygen mole fraction (H0O0).

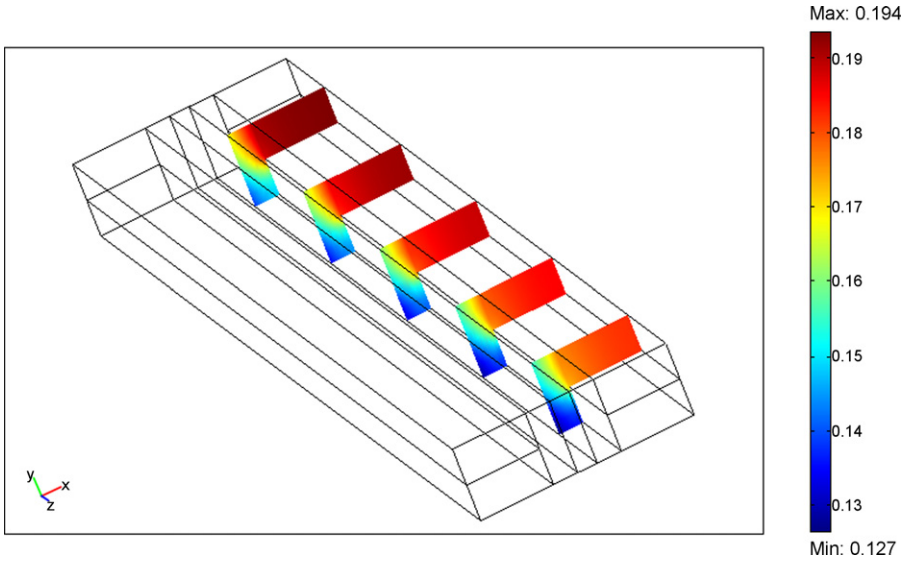

Fig. 12. Oxygen mole fraction (H2O2, H2O3, H3O3).

6. Conclusions

Analytical solutions were presented for the transport and electrochemical problem in PEM fuel cell catalyst layers at both the anode and cathode. These solutions transformed the volumetric reaction terms to boundary fluxes, thereby eliminating the need to mesh the catalyst layer. The result was a model that required less computational memory and converged in less time.

These semi-analytical solutions matched very well with a full computational model in terms of the polarization results, hydrogen and oxygen concentration. The results showed that the analytical techniques did not compromise the accuracy of the model. It was further suggested that these techniques could reduce the computational requirements of 2D transport models, whereby allowing them to be incorporated into system models.

The techniques presented in this paper applied primarily to high temperature PEM fuel cells, using alternative membranes to Nafion®, e.g. PBI.

References

[1] D.M. Bernardi, M.W. Verbrugge, J. Electrochem. Soc. 139 (9) (1992) 2477–2491.
[2] V. Gurau, H. Liu, S. Kakac, AIChE J. 44 (1998) 2410–2422.
[3] T. Berning, N. Djilali, J. Power Sources 124 (2003) 440–452.
[4] M. Hu, A. Gu, M. Wang, X. Zhu, L. Yu, Energy Convers. Manage. 45 (2004) 1861–1882.
[5] S. Ge, B. Yi, J. Power Sources 124 (2003) 1–11.
[6] P.T. Nguyen, T. Berning, N. Djilali, J. Power Sources 130 (2004) 149–157.
[7] S. Um, C.Y. Wang, J. Power Sources 125 (2004) 40–51.
[8] N.P. Siegel, M.W. Ellis, D.J. Nelson, M.R. Spakovsky, J. Power Sources 128 (2004) 173–184.
[9] D.F. Cheddie, N.D.H. Munroe, Energy Convers. Manage. 47 (2006) 1490–1504.
[10] D.F. Cheddie, N.D.H. Munroe, J. Power Sources 156 (2006) 414–423.
[11] D.F. Cheddie, N.D.H. Munroe, Int. J. Transp. Phenom. 8 (2006) 51–68.
[12] D.F. Cheddie, N.D.H. Munroe, J. Power Sources 160 (2006) 215–223.
[13] D.F. Cheddie, N.D.H. Munroe, Int. J. Hydrogen Energy 32 (2007) 832–841.
[14] A.R. Korsgaard, R. Refshauge, M.P. Nielsen, M. Bang, S.K. Kaer, J. Power Sources 162 (2006) 239–245.
[15] J. Hu, H. Zhang, J. Hu, Y. Zhai, B. Yi, J. Power Sources 160 (2006) 1026–1034.
[16] J. Hu, H. Zhang, L. Gang, Energy Convers. Manage. 49 (2008) 1019–1027.
[17] C.H. Li, X.J. Zhu, G.Y. Cao, S. Sui, M.R. Hu, J. Power Sources 175 (2008) 303–316.
[18] D.F. Cheddie, N.D.H. Munroe, J. Power Sources 171 (2007) 634–643.
[19] X. Xue, J. Tang, A. Smirnova, R. England, N. Sammes, J. Power Sources 133 (2004) 188–204.
[20] F. Standaert, K. Hemmes, N. Woudstra, J. Power Sources 63 (1996) 212–234.
[21] F. Standaert, K. Hemmes, N. Woudstra, J. Power Sources 70 (1998) 181–189.
[22] L. Pisani, Int. J. Heat Mass Transfer 51 (2008) 650–660.
[23] Y.T. Lin, C.T. Lin, Y.C. Chen, K.M. Yin, C.T. Yang, Int. J. Hydrogen Energy 32 (2007) 4477–4488.
[24] A.A. Kulikovsky, Electrochem. Acta 53 (2007) 1353–1359.
[25] M. Eikerling, A.A. Kornyshev, J. Electroanal. Chem. 453 (1998) 89–106.
[26] S. Litster, N. Djilali, Electrochem. Solid State Lett. 11 (2008) B1–B5.